Helsinki Conference Proceedings 2019, R. Holmberg et al

Joints mapping with commercial monitoring tools - techniques, results and lessons

P. Segarra, J.A. Sanchidrián, A.P. Perez, J. Navarro & C. Paredes
Universidad Politécnica de Madrid – E.T.S.I. Minas y Energía. Madrid, Spain.

ABSTRACT: The intersections of discontinuities with the rock face have been assessed in two quarry blasts through photogrammetry. Geotechnical conditions within the rock mass are also investigated from 2D oriented photographs of the blasthole walls from measurements with optical televiewer in the same blasts. One operator manually analysed the in-hole photographs, while two mapped manually discontinuities in the 3D photogrammetric models. The orientation of discontinuities and spacing between them are discussed and applied to assess the rock factor in the xp-frag model. Uncertainty in rock mass characteristics due to the measuring conditions is assessed and their effect on the resulting fragmentation assuming constant blasting parameters discussed. The bias due to the operator leads to a moderate relative difference in fragmentation of about ±15%, while the effect of the monitoring tool, sampling direction and image scale involves significant changes in fragmentation; photogrammetry provides coarser fragmentation than televiewer by a factor of 1.38 to 2.45, depending on the percentile considered.

1 INTRODUCTION

Pre-existing discontinuities in the rock mass, such as bedding planes, primary foliation, planes of schistosity, fractures or joints, define a system of rock blocks (Palmström 2001) that have a large influence in the results of bench blasting, such as over-excavation, toe breakage, pit floor conditions, fragmentation and rock motion from bench blasting (AECI 1983, Ash 1968, Burkle 1979, Hustrulid 1999).

The orientation (i.e. dip and dip direction) of the predominant discontinuities with respect to the free face of the blast and their spacing have been rated to assess the blastability of the rock (Lilly 1986 & 1992) and to predict the median size through the modified Kuznetsov equation in the Kuz-Ram model (Cunningham 1987& 2005, Kuznetsov 1973). These geotechnical conditions are also considered on the xp-frag distribution-free model (Sanchidrián & Ouchterlony 2017) developed recently as an alternative to classical models like Kuz–Ram and crush-zone (Kanchibotla *et al*. 1999, Thornton *et al.* 2001) that rely on the Rosin-Rammler distribution (Rosin & Rammler 1933, Weibull 1939 & 1951).

Rock mass conditions are commonly assessed from the properties of the fractures (orientation and spacing) intersected by horizontal and vertical scanlines on the rock face of the bench (Hamdi &

du Mouza 2005, ISRM 1978, Priest & Hudson 1981, Svahn 2003). In the last years, the use of terrestrial digital photogrammetry and laser scanning has been extended to investigate rock mass properties in blasting (Beyglou *et al.* 2015; Kemeny & Handy 2004, Ouchterlony *et al.* 2010).

Recent published works have validated these techniques from *in situ* measurements in rock outcrops near infrastructures (Osterman 2017, Drews *et al.* 2018). However, the uncertainty in both orientation and spacing of the discontinuities (and thus in the blastability index and predicted fragmentation) due to the tools limitations and setup, the sampled area of the rock mass (free face or blasthole) and the operator bias has been little investigated. To bridge this gap, pre-blast conditions have been monitored using photogrammetry and optical televiewer within the European Union-funded project SLIM (Sanchidrián 2018, SLIM 2019). Photogrammetry is a mature technology commonly used in bench blasting, while no references to the use of optical televiewer to assess pre-blast rock conditions, have been found by the authors.

2 THE SITE

The experimental work was carried out at El Aljibe quarry owned by Benito Arnó e Hijos. The quarry is located near the town of Almonacid de Toledo (Spain) and mines mylonite to produce among other aggregate materials, track ballast for high-speed and conventional trains. The rock has a density of 2721 kg/m^3 and an average uniaxial compressive strength of 171sd.79 MPa (Castedo *et al.* 2018).

The rock structure can be described as blocky. One subhorizontal family and 2 to 4 subvertical sets are detected from *in situ* measurements at the deepest level of the pit. The subhorizontal family is related to the Hercynian normal fault of Montes de Toledo, which originated the main foliation of the mylonites (Enrile 1991), while the subvertical sets are related with the oblique movement of the fault's blocks in the last tectonic episodes of the Hercynian Orogeny (Barbero *et al*. 2005).

The blasts were located one behind each other in the Southwest part of the deepest pit level. They consisted of one row with seven blast-holes drilled with 89 mm diameter and a nominal inclination of 15°; more details on the blasts are given in Segarra *et al.* (2018). The dip direction of the bench face was towards SW, with a dip about 70°, and a mean height of 11.5 m.

3 PHOTOGRAMMETRY

In each block, six photographs of the free face were taken from the grade level at 30 m from the toe. The photos were made parallel to the rock face with a separation of about 5 m. A calibrated camera Canon EOS 70D with 20 Mpx and a Tamron 17 mm zoom was used. Six to eight disc targets were placed along the toe of the highwall and two additional ones were placed at the top part on the lateral limits of the block. The 3D model is georeferenced from the absolute coordinates of the discs obtained with a Quarryman ALS laser system.

The software ShapeMetriX 3D-SMX (3GSM, 2010) was used to process the photos and analyse the data. The bench surface analysed was 304 m^2 for blast B1 and 270 m^2 for blast B2. The average 3D spacing between points was 6 cm.

In order to address the human bias, two operators have manually mapped the discontinuities in the 3D models of both blasts. Operator 1 (Op1) was an experienced geologist

Table 1. Total number of discontinuities and percentage assigned and not assigned to a cluster (in each cell, the first number corresponds to PhOp1 analysis, the second to PhOp2 and the third to TvOp1).

Blast	Number of joints	Percentage					
		Sh	SvSW	SvS/SE	SvE/SE	SvNE	NA
B1	94a/168b/160c	30/35/38	24/21/18	32/28/14	- / - /14	- / -/13	14/17/3
B2	67 /156 /77	35/28/14-30	22/26/ -	- /29/23	24/ - /14	-/ -/16	19/17/3

Key - a:PhOp1; b:PhOp2; c:TvOp1.

Ph: photogrammetry; Tv: televiewer. Sh: Subhorizontal set; SvSW= Subvertical set in SW direction; SvS/SE= Subvertical set in S/SE; SvE/SE= Subvertical set in E/SE; SvNE=subvertical set in NE; NA: not assigned to any cluster.

while Operator 2 (Op2) had little experience and followed basic guidelines provided by Operator 1. Op1 spent two hours per blast and Op2 four hours. Both operators used a 1.5 m squared grid to map the relevant structures close to the grid lines. Few planes (or facets) of discontinuities were apparent in the rock face and discontinuities were usually defined by a polygonal line that follows the trace of the discontinuities in 3D space; Op1 used a single long line to map the discontinuity trace, while Op2 traced several short lines to map the same discontinuity. This results in more discontinuities from the analysis by Op2 (see the first and second figures in the second column of Table 1).

4 OPTICAL TELEVIEWER

The geotechnical condition of the blastholes was analysed with an optical televiewer manufactured by Advanced Logic Technology. This system is composed by a QL40 OBI-2G logging tool (1470 × 40 mm) with a digital image sensor at the bottom with an active pixel array of 1.2 Mpx and fisheye matching optics. The logging tool has also 10 LEDs to light the hole walls and hole deviation sensors. Two centralisers are mounted at the top and bottom parts of the tool to ensure that it is well centred in the hole. The monitoring device is completed with a data acquisition system (BBox), a mini-winch with 200 m of wireline that pulls the logging tool at constant velocity, powers it and allows data exchange. A computer to control the tool and record the images is required.

The assembly of this equipment in the field takes a minimum of 30 minutes. Five and three blastholes were monitored from bottom to top in blasts B1 and B2, respectively; the upper 1.5 m that correspond to the length of the logging tool cannot be measured. The azimuthal resolution was set to 900 px and the vertical resolution was 1 mm. About 45 minutes were spent per hole for these conditions (the monitored length of the holes ranged from 11 to 12.8 m).

The televiewer provides for each blasthole, a continuous unwrapped 360˚ oriented colour (2D) image of the hole walls. In this image, discontinuities appear as sinusoidal traces from which features (amplitude, and the coordinates of three non-collinear points), it is possible to calculate their dip, dip direction and aperture (Li *et al.* 2013, Wang *et al.* 2002, Williams & Johnson 2004). Wellcad software (ALT 2017) was used to analyse the in-hole photographs. Although the software maps discontinuities automatically, the performance of this analysis was poor since too many discontinuities were marked, and a manual mapping of the logs was made by Operator 1. To reduce the bias in the analysis, a library of the fractures and structures to be marked was defined, namely: open (continuous) fracture, continuous closed fracture, discontinuous fracture (its trace is not continuous and it is visible in 50 to 75 % of the lateral surface of the hole wall), filled fracture, and voids (Gomes *et al.* 2018). The latter was considered only for the spacing calculation, while internal structures of the rock, such as foliation and mineralised veins were not considered.

5 ANALYSIS OF RESULTS

Geotechnical conditions for each blast are obtained from three analyses in which two monitoring tools to sample rock mass discontinuities at different locations and two operators were involved. The measuring conditions are (in brackets the short name given): photogrammetry analysed by Op1 1 and Op2 (PhOp1 and PhOp2, respectively) and televiewer mapped by Op1 (TvOp1). Although these tools provide other data in addition to orientation and spacing of discontinuities, only these parameters are analysed here.

5.1 Orientation of discontinuities

In order to explore the concentration of discontinuities resulting from each analysis, and to preliminary explore the sets or families present in the rock mass, the intensity of poles is calculated. For this purpose, the gathering degree is calculated for every j^{th} discontinuity as follows (Ma *et al.* 2015):

$$\varphi_j = \sum_{i=1}^{n} \cos\theta_{ij} \quad (1)$$

where θ_{ij} is the angular distance between the unit normal vectors U_i and V_j of discontinuities i and j obtained as $\cos^{-1}(|U_i \bullet V_j|)$ and n is the number of discontinuities at a distance smaller or equal than the gathering degree threshold, Ω ($\theta_{ij} \leq \Omega = 20^\circ$; a range from 5 to 20˚ is suggested by Ma *et al.* (2015).

For each discontinuity, φ_j accounts for both the number of fractures around it and the distance to it (i.e. high values of φ_j correspond to high density

of discontinuities). Figure 1 shows in a different plot the gathering density contours of discontinuities for each blast and analysis type; a lower hemisphere of an equal area stereographic projection has been considered. The values assigned to the colours of the contours are kept constant for every analysis and plots without the lightest shade areas indicates that less discontinuities were mapped (see second column in Table 1). In each graph, areas with the lightest shades show orientations with higher density of discontinuities than darkest shaded areas.

Non shaded zones of the stereonets in Figure 1 correspond to orientations in which no discontinuities were measured. The dip of discontinuities from televiewer logs (top and bottom right graphs, Figure 1) is smaller than from photogrammetry; such result is caused by the difficulty of measuring the amplitude of the sinusoidal traces associated to vertical joints.

In blast B1, the orientations with high density of fractures are similar for photogrammetry models analysed by Op1 and Op2 (see left and central top graphs for PhOp1 and PhOp2, Figure 1), while optical televiewer (right top graph, Figure 1) provides subvertical sets at different orientations (see mid-toned areas in the E and NE directions) with the exception of subhorizontal discontinuities. In blast B2, differences between each analysis are larger, especially for the subvertical joints, (see bottom graphs in Figure 1). These are oriented towards E/SE direction in PhOp1 analysis (left bottom graph, Figure 1), concentrated around the S for PhOp2 (central bottom graph, Figure 1) and in the S/SE and NE directions for TvOp1 (right bottom graph, Figure 1).

Figure 2 shows the normal of the mapped discontinuities for each blast in the lower hemisphere of an equal angle stereographic projection; a different shade is used to differentiate each analysis type. The discontinuities from each analysis were not coincident in most of the cases. To cluster the discontinuities from photogrammetry (PhOp1 and PhOP2 analyses), the software ShapemetriX has been used; the number of sets or clusters was fixed to three according to Figure 1 and the maximum membership angle (it accounts for uncertainty within the data) has been set to 35˚ according to 3GSM experience (smaller angles leave outside the clusters a large number of discontinuities).

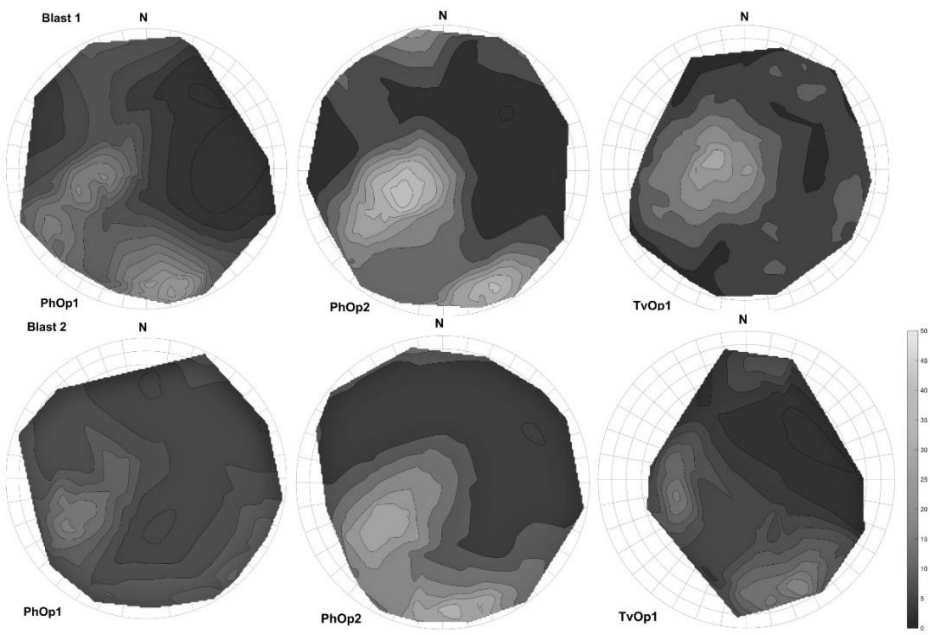

Figure 1. Gathering density contours of discontinuities (Ω=20˚) from each analysis type (PhOp1, PhOp2, TvOp1) and blast (B1 and B2).

MATLAB (2015) is used to cluster discontinuities from televiewer logs (TvOp1 analysis); the function *kmeans* has been adapted to consider the angular distance proposed by Hammah and Curran (1998):

$$d^2(U_i, V_j) = 1 - (U_i \bullet V_j)^2 \quad (2)$$

The same membership angle used previously was considered, while the number of clusters has been increased to five.

A Fisher distribution (Fisher 1953) has been used to plot the resulting clusters in Figure 2; in each set, the mean orientation of the normal vector is shown by a cross; the 95 % cone of confidence (i.e. a region around the mean direction of the discontinuity set where there is a 95 % probability of the mean orientation to fall) is given with a thick line, and the spherical aperture (i.e. an estimate of the standard deviation in the orientation of the discontinuities assigned to the set) is given by a thin line.

One subhorizontal (Sh) and four subvertical sets in Soutwest (SvSW), South-Southeast (SvS/SE), East-Southeast (SvE/SE) and Northeast (SvNE) directions are identified in both blasts by at least one of the analyses. Table 1 shows the percentage of discontinuities assigned to each cluster and the percentage not clustered.

Only the subhorizontal set (Sh) is identified in all three analyses in both blasts; in blast B2, however, two subhorizontal sets are obtained from in-hole photographs (see lighter shaded circles near the centre of right graph). In blast B1, all three analyses show a discontinuity set in SW and S/SE directions, while the other two discontinuity sets in E/SE and NE directions are only detected by televiewer analysis. In blast B2, the subvertical sets observed depend on the measuring conditions. For instance, in the analysis of the photogrammetry model, discontinuity SvS/SE is only observed by Op2, while the set in the SW direction is only detected by Op1. For these two analyses (PhOp1 and PhOp2), few sets are mapped in the North directions, and no cluster is obtained from televiewer logs.

The angular distances between the mean unit normal vectors of the clusters obtained at similar directions, and thus showing the same discontinuity set, are shown in Table 2; the horizontal set towards the S direction, detected only with televiewer in blast B2, is discarded for the analysis. These distances describe the uncertainty in the mean orientation of the family sets from the different analysis types and are given in bold when no differences between the mean unit vectors can be stated at a level of 95 %, i.e. their cones of confidence overlap (thick lines in Figure 2). This occurs in 4 pairs out of 15. The angular distances are below the maximum membership

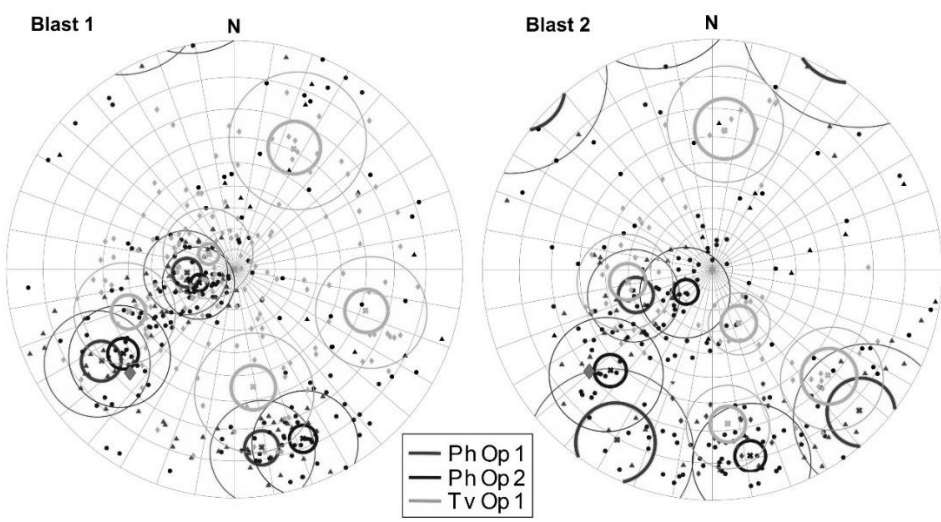

Figure 2. Cluster analysis of the joints mapped with photogrammetry by operators 1 (PhOp1) and 2 (PhOp2, darkest shade) and Optical televiewer by Operator 1 (TvOp1, lightest shade) for blasts B1 and B2.

Table 2. Angular distances (in degrees) between unit normal vectors of the clusters of the same discontinuity set obtained with different analyses.

Blast	Analysis	Sh	SvSW	SvS/SE	SvE/SE	SvNE
B1	PhOp1 - PhOp2	7.7	8.0	13.0	-	-
	PhOp1 - TvOp1	14.7	23.0	24.5	-	-
	PhOp2 - TvOp1	14.5	17.9	27.0	-	-
B2	PhOp1 - PhOp2	23.4	22.7	-	-	-
	PhOp1 - TvOp1	6.3	-	-	16.1	-
	PhOp2 - TvOp1	27.1	-	14.9	-	-

angle of 35˚ considered to cluster the joints, and the mean and standard deviation of the distances are 17.9˚ and 7˚, respectively.

The normal direction of the rock face in both blasts is shown with a mid-toned diamond in Figure 2 to assess Lilly's orientation index j_0 that shows the relative difficulty degree of the blast to break the toe. Sanchidrián & Ouchterlony (2017) have normalized this index so that it is 0.25 for horizontal discontinuities, 0.5 for dipping out of the face, 0.75 for sub-vertical discontinuities striking normal to the face and 1 for dipping into the face or no visible jointing. No value is assigned to j_0 for discontinuities, like the SW set (see Figure 2), that are nearly parallel to the face; since this situation involves a poor performance of the explosive, the highest rating (j_0=1) is considered.

One approach to assess the orientation index is to consider only the discontinuity set that favours fragmentations and leads, then, to a smaller j_0. This is the case of the subhorizontal joints identified by all three analyses in both blasts and therefore no differences in j_0 can be attributed to the measuring and analysis conditions. As an alternative, all the discontinuities can be considered to calculate j_0 (Soft-Blast 2006). Orientations of the normal directions of all discontinuities and of the face are the inputs and the process consists of: i) assigning an orientation index j_{0i} to each i –discontinuity according to an algorithm with four conditions (Bernardini 2019, Yi *et al.* 2018); and ii) calculating the mean of the j_{0i} values. The resulting mean j_0 values for each blast and analysis are shown in Table 3.

Since subvertical joints detected in El Aljibe hamper toe breakage, the resulting j_0 values are greater than when only the horizontal set is considered. The j_0 values for blast B1 range from 0.55 to 0.64, while they are higher for blast B2, 0.62 to 0.69. The variability (or standard deviation) of j_0 values within each blast and analysis set is nearly constant, about 0.25 and the uncertainty between different analysis types, expressed as the ratio of the standard deviation to the mean of the j_0, is limited in both blasts to about 6 %.

Table 3. Overall rock orientation index j0.

Blast	Analysis	Mean	Std
B1	PhOp1	0.64	0.24
	PhOp2	0.58	0.25
	TvOp1	0.55	0.27
B2	PhOp1	0.69	0.24
	PhOp2	0.62	0.23
	TvOp1	0.62	0.22

5.2 Spacing analysis

The spacing between discontinuities in photogrammetry analyses (PhOp1 and PhOp2) is obtained from three horizontal scanlines defined in the 3D model in which the mapped discontinuities were imported; the scanlines cover the whole free face and divide the bench height into four equal parts. The use of vertical scanlines was discarded since they were crossed by few discontinuities, mainly the subhorizontal ones.

For televiewer data, the spacing between discontinuities is calculated from the distance between the centre of the adjacent discontinuities

or voids mapped in each blasthole; in this case, the blasthole direction and dip (36–60° and 13–22°, respectively) defines a different sampling direction. The cumulative distribution functions of the observed spacing are plotted in Figure 3; the same shading as used for each analysis in Figure 2 are used here. Results from blast B1 are plotted with continuous lines, and dashed lines are used for B2.

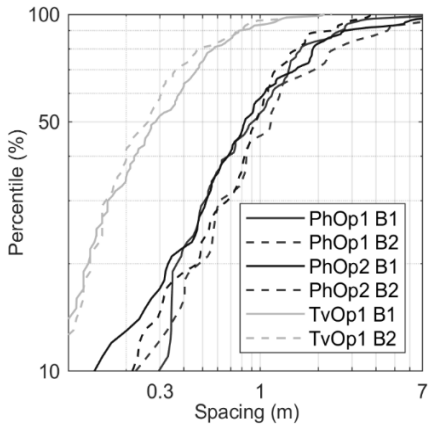

Figure 3. Empirical cumulative distributions of discontinuity spacing.

In order to assess differences between the cumulative distributions between each pair of analysis types for each blast, a two-sample Kolmogorov-Smirnov test has been applied. It shows that no statistical differences can be assessed between analysis of photogrammetry by both operators (PhOp1 and PhOp2 Figure 3) in both blasts at a confidence level of 97%; the p-values are 0.67 and 0.03 for blasts B1 and B2, respectively. The distributions from in-hole data (TvOp1) and from photogrammetry (either PhOp1or PhOp2) are significantly different; the p-values are well below 10^{-3}.

These results suggest a limited effect of the operator in the joints spacing in comparison with the measuring method (photogrammetry versus televiewer). The latter also encompasses differences in the sampling direction and in the image scale since discontinuities from in-hole photographs are sampled at significantly closer distances than photogrammetry, and it is then more probable to sample more discontinuities per meter with optical televiewer. In fact, distributions from televiewer analysis (in Figure 3) are shifted towards smaller spacing than distributions from photogrammetry in both blasts. The median joints spacing s_{j50} of televiewer analyses in both blasts is near 0.3 m (see s_{j50} in Table 4) which is a moderate spacing (0.2–0.6 m; ISRM, 1978), while the spacing from photogrammetry trebles these values, and the spacing can be ranked qualitatively as wide (0.6–2 m) (ISRM 1978). Table 4 provides the spacing at percentiles 30, 80 and 100 ($s_{j\max}$).

Table 4. Spacing between discontinuities (in m) at different percentiles.

Blast	Analysis	s20	s50	s80	smax
B1	PhOp1	0.37	0.91	1.62	1.30
	PhOp2	0.33	0.83	1.88	2.01
	TvOp1	0.13	0.28	0.57	0.38
B2	PhOp1	0.48	1.13	2.45	2.00
	PhOp2	0.47	0.94	1.56	0.82
	TvOp1	0.13	0.26	0.48	0.37

6 DISCUSSION

The mean orientation index (j_0) and the median spacing between discontinuities (s_{j50}) shown in Tables 3 and 4, respectively, are used to assess the blastability index or joint factor J_F defined in the xp-frag model. This is given as function of the percentile P as follows:

$$J_F = J_S + J_0 = \min\left(\frac{s_{j50}}{B}, a_s\right) + j_0 a_0 \qquad (3)$$

where B is the burden and a_s and a_0 are model parameters that depend on the percentile P through functional forms defined for percentiles 5 to 100; these formulae are not given here for simplicity but they can be found in the original paper by Sanchidrián and Ouchterlony (2017).

Figure 4 shows the joint factor J_F as function of the percentile for each analysis type and blast; the nominal burden of the blasts studied is used, B=2.6 m.

The term J_s in Equation (3) is equal to S_{j50}/B for all the data sets since S_{j50}/B is smaller than a_s for all percentiles. The differences in the rock factor between each analysis type increase as the percentile does. The effect of the operator (comparison of PhOp1, and PhOP2) is minor and Op2 leads to a slightly lower rock factors in both

blasts. The effect of the measuring tool is much larger, and smaller rock factors at each percentile are obtained from televiewer data in both blasts (see curves for TvOp1); the significantly different spacing between discontinuities obtained from this analysis (see TvOp1 curves in Figure 3) is likely behind this result.

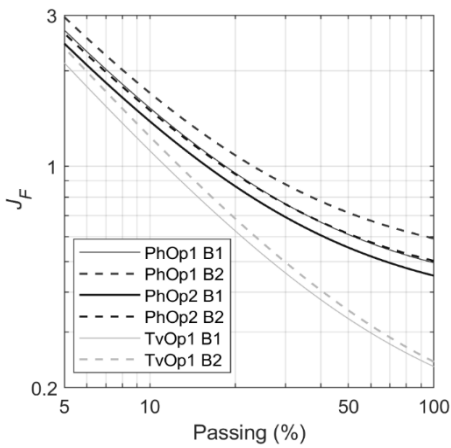

Figure 4. Joint Factor (J_F) versus percentage passing.

Table 5. Relative difference in the rock factor J_F between each pair of analysis.

Blast	Analysis	Percentile			
		20	50	80	100
B1	PhOp1 / PhOp2	1.10	1.10	1.10	1.10
	PhOp1 / TvOp1	1.52	1.84	2.04	2.13
	PhOp2 / TvOp1	1.38	1.68	1.85	1.94
B2	PhOp1 / PhOp2	1.15	1.17	1.17	1.18
	PhOp1 / TvOp1	1.59	2.03	2.32	2.45
	PhOp2 / TvOp1	1.38	1.75	1.97	2.08

If the blast characteristics are assumed constant, the ratio between the joint factors for different analyses describe relative differences in the resulting fragmentation. These ratios are shown in Table 5 for percentiles 20, 50, 80 and 100. Rock size distributions predicted with photogrammetry data from two operators (PhOp1/PhOp2) show a moderate relative difference of about ±15% in both blasts. Such difference is significantly higher when different methods are considered (PhOp1/TvOp1 and PhOp2/TvOp1), and fragmentation predicted using photogrammetry is, depending on the percentile, 1.38 to 2.45 higher than that from televiewer.

7 CONCLUSIONS

The intersections of discontinuities with the rock face and with eight blastholes were monitored with photogrammetry and optical televiewer, respectively, in two blasts at a mylonite quarry. Discontinuities in the 3D photogrammetry model have been mapped manually by two operators, while those in the 2D in-hole photographs were mapped by one operator. The main geotechnical characteristics, orientation of discontinuities and spacing between them have been obtained from each of these three analyses.

For each analysis, the resulting number and orientation of discontinuities is different, involving differences in the resulting sets of discontinuities from cluster analyses. Only one set of discontinuities, that is nearly horizontal, has been detected in both blasts by all analyses. The number and orientation of the other sets of discontinuities that are nearly vertical, vary for different analyses. Large differences are found between photogrammetry and optical televiewer, leading to three and five discontinuity sets, respectively, in both blasts.

A procedure to calculate Lilly's orientation index based on the orientation of all discontinuities without the need of clustering has been developed. Variability in the resulting index between analyses is limited in both blasts, about 6% of the mean.

In photogrammetric models, the spacing between discontinuities has been assessed from three horizontal scanlines of about 25 m, covering the complete free face. For televiewer data, the blasthole defines the scanline along which the discontinuity spacing has been assessed. The effect of the operator in the results from photogrammetry does not produce significant differences in the spacing distributions. On the contrary, these are

significantly different between measurements on the bench face with photogrammetry and the blastholes with televiewer; the resulting median spacings are about 0.9 and 0.3 m, respectively, in both blasts.

The effect of the operator on the blastability index, or joints factor, of the xp-frag model is minor compared to the variability of the different tools. If blast characteristics are assumed constant, the relative difference in the predicted fragmentation when the rock factor is built from photogrammetry data from two operators is about ±15%. Fragmentation predicted from photogrammetry based joint factor is 1.38 to 2.45 (depending on the percentile) coarser than considering the televiewer based factor. Results from all the blasts monitored during the project are under analysis to improve the quantitative significance of the results.

8 ACKNOWLEDGMENTS

This work has been conducted under the SLIM project funded by the European Union's Horizon 2020 research and innovation program under grant agreement no. 730294. The involvement of the technical staff of El Aljibe quarry during the field campaign is acknowledged. We would also like to express our gratitude to MAXAM Terra Solutions for their cooperation and support. The help and contribution of the students involved in the work is also recognised.

REFERENCES

3GSM 2010. 3D imaging for measuring and assessing rock and terrain surfaces. *Shape-Metrix3D user manual* – 3GSM, Austria. 2010.

AECI 1983. Geology and fragmentation. In *Explosives Today-Technical Bulletin*, series 2, No.34. African Explosives and Chemical Industries (AECI). Johannesburg.

ALT 2017. WellCAD software 5.1, Version TK160126. Advanced Logic Technology.

Ash, R.L. 1968. The design of blasting rounds. In E.P. Pfleider (ed.) *Surface mining*. The American Institute of Mining, Metallurgical, and Petroleum Engineers: Englewood, CO, USA

Barbero, L., Glasmacher, U.A., Villaseca, C., García, J.L. & Martín-Romera, C. 2005. Long-term thermo-tectonic evolution of the Montes de Toledo area (Central Hercynian Belt, Spain): constraints from apatite fission-track analysis. *International Journal of Earth Sciences* 94(2): 193-203.

Beyglou, A., Schunnesson, H., Johansson, D. & Johansson, N. 2015. Adjusting initiation direction to domains of rock mass discontinuities in Aitik open pit mine. *International Symposium on Rock Fragmentation by Blasting*, 24-25 August. The Australasian Institute of Mining and Metallurgy. Carlton, pp. 385-391.

Bernardini, M. 2019. Application of LiDAR and photogrammetry methods at El Aljibe quarry (Toledo, Spain) to characterise the rock mass for fragmentation prediction in rock blasting through Kuz-Ram and xp-frag models. *Master Thesis*. Politecnico de Torino: Turin.

Burkle, W.C. 1979. Geology and its effect on blasting. *Proceedings of the Annual Conference on Explosives and Blasting Technique 5th Annual Meeting*, 7-9 February 1979. International Society of Explosives Engineers: Cleveland, pp 105-120.

Castedo, R., Pérez-Fortes, P. & Segarra, P. 2018. Collection of rock samples in El Aljibe. Mechanical characterisation of rock mass, version 1.1. *SLIM Technical Report, European Union's Horizon 2020 research and innovation program under grant agreement No. 730294*. Universidad Politécnica de Madrid: Madrid.

Cunningham, C.V.B. 1987. Fragmentation estimations and the Kuz-Ram model—four years on. In: Fourney WL, Dick RD (eds): *Proceedings of 2nd international symposium on rock fragmentation by blasting*, 23–26 August 1987. Society of Experimental Mechanics, Bethel, pp 475–487.

Cunningham, C.V.B. 2005. The Kuz–Ram fragmentation model–20 years on. In R. Homberg et al. (eds.): *Proceedings of 3rd world conference on explosives and blasting*, 13-16 Sept. European Federation of Explosives Engineers: Kolmården, Sweden, pp 201–210.

Drews, T., Miernik, G., Anders, K., Höfle, B., Profe, J., Emmerich, A. & Bechstädt, T. 2018). Validation of fracture data recognition in rock masses by automated plane detection in 3D point clouds. *International Journal of Rock*

Mechanics and Mining Sciences 109: 19-31.

Enrile, J. H. 1991. Extensional tectonics of the Toledo ductile-brittle shear zone, central Iberian Massif. *Tectonophysics* 191(3-4): 311-324.

Fisher, R.A. 1953. Dispersion on a sphere. *Proceedings of the Royal Society of London. Series A. Mathematical and Physical Sciences* 217(1130), 295-305.

Gomes, T., Segarra, P., Natale, M. & Pérez-Fortes, A. P. 2018. El Aljibe tests blasts-2018. Procedure for rock mass characterization with optical televiewer V 1.1. *SLIM Technical Report, European Union's Horizon 2020 research and innovation program under grant agreement No. 730294*. Universidad Politécnica de Madrid: Madrid.

Hammah, R. E. & Curran, J. H. 1998. Fuzzy cluster algorithm for the automatic identification of joint sets. *International Journal of Rock Mechanics and Mining Science*s 35(7): 889-905.

Hamdi, E. & du Mouza, J. 2005. A methodology for rock mass characterisation and classification to improve blast results. *International Journal of Rock Mechanics and Mining Sciences* 42(2): 177-194.

Hustrulid, W. 1999. Blasting principles for open pit mining. *Vol I general design concepts*. CRC Press: Boca Raton, pp 97-101.

ISRM 1978. Suggested methods for the quantitative description of discontinuities in rock masses. Barton, N. (working group co-ordinator). *International Journal of Rock Mechanics and Mining Sciences & Geomechanics Abstracts*. International Society of Rock Mechanics. 15(6): 319-369.

Kanchibotla, S.S., Valery, W. & Morrell, S. 1999. Modelling fines in blast fragmentation and its impact on crushing and grinding. *Proceedings of Explo'99—a conference on rock breaking*, 7-11 Nov. The Australasian Institute of Mining and Metallurgy: Carlton, pp 137-144.

Kemeny, J. & Handy, J. 2004. Improving blast fragmentation prediction with new technologies for rock mass characterisation. *Proceedings of the 30th Annual Conference on Explosives and Blasting Technique*, 1-4 February. International Society of Explosives Engineers: Cleveland, pp. 291-300.

Kuznetsov, V.M. 1973. The mean diameter of the fragments formed by blasting rock. *Soviet Mining Science* 9:144–148.

Li, S.J., Feng, X.T., Wang, C.Y. & Hudson, J.A. 2013. ISRM suggested method for rock fractures observations using a borehole digital optical televiewer. *Rock mechanics and rock engineering* 46(3): 635-644.

Lilly, P.A. 1986. An empirical method of assessing rock mass blastability. Davidson, J.R. (ed.) *Proceedings of large open pit mine conference*, October 1986. The Australasian Institute of Mining and Metallurgy: Parkville, pp 89–92.

Lilly, P.A. 1992. The use of blastability index in the design of blasts for open pit mines. T. Szwedzicki, G.R. Baird, T.N. Little (eds.), *Proceedings of Western Australian conference on mining geomechanics*, 8-9 June 1992. Western Australia School of Mines: Kalgoorlie, pp 421-426.

Ma, G.W., Xu, Z.H., Zhang, W. & Li, S.C. 2015. An enriched K-means clustering method for grouping fractures with meliorated initial centres. *Arabian Journal of Geosciences* 8(4): 1881-1893.

MATLAB Release 2015b, 2015, The MathWorks, Inc., Massachusetts.

Osterman, F. 2017. Comparison of Photogrammetry Interpretation with Physical Structural Field Measurements. Independent project of the Department of Earth Sciences. Uppsala University: Uppsala.

Ouchterlony, F., Nyberg, U., Olsson, M., Vikström, K., Svedensten, P. & Bergskolan i Filipstad. 2010. Optimal fragmentering i krosstäkter, fältförsök i Långåsen. *Swebrec report 2010:2*. Swedish Blasting Research Centre: Luleå University of Technology. In Swedish.

Palmström, A. 2001. Measurement and characterisation of rock mass jointing. In Sharma VM & Saxena KR (eds.): *In-situ characterization of rocks*. Lise: Balkema, 49-97.

Priest, S.D. & Hudson, J.A. 1981. Estimation of discontinuity spacing and trace length using

scanline surveys. *International Journal of Rock Mechanics and Mining Sciences & Geomechanics Abstracts* 18(3): 183-197.

Rosin, P. & Rammler, E. 1933. The laws governing the fineness of powdered coal. *Journal of the Institute of Fuel* 7:29–36.

Sanchidrián, J.A. 2018. SLIM: Technology for blasting to improve mining. *In: 12th International Symposium on Rock Fragmentation by Blasting, Luleå, Sweden*, 783-793.

Sanchidrián, J.A. & Ouchterlony, F. 2017. A distribution-free description of fragmentation by blasting based on dimensional analysis. *Rock Mechanics and Rock Engineering* 50(4), 781-806.

Segarra, P., Sanchidrián, J.A., Castedo, R., Pérez Fortés, A.P., Iglesias, L., Fernández, A., Navarro, J., Johansson, D., Stenman, U., Thurley, M. & Nyberg, U. 2018. Controlling rock fragment Size distribution: large and Small-scale testing. *SLIM Deliverable Report D2.3*, European Union's Horizon 2020 research and innovation program, Grant agreement no. 730294.

Soft-Blast 2006. JKSimBlast blast simulation evaluation and management. *User Manual*. JKTech and JKMRC Technology Transfer, University of Queensland, Australia.

SLIM 2019, April. Sustainable Low Impact Mining solution for exploitation of small mineral deposits based on advanced rock blasting and environmental technologies *European H2020 funded Projec*t.

Svahn, V. 2003. Generation of fines in bench blasting. *Licentiate Thesis*. Chalmers University of Technology: Göteborg, Sweden.

Thornton, D., Kanchibotla, S.S. & Brunton, I. 2001. Modelling the impact of rock mass and blast design variation on blast fragmentation. In: *Proceedings of Explo 2001*, 28-31 October 2001. The Australasian Institute of Mining and Metallurgy: Carlton, pp 197-205.

Wang, C.Y., Law, K.T., Sheng, Q. & Ge, X.R. 2002. Borehole camera technology and its application in the Three Gorges project. *Proceedings of the 55th Canadian geotechnical and 3rd joint IAH-CNC and CGS groundwater specialty conferences*, Niagara Falls, Ontario (pp. 601-608).

Weibull, W. 1939. A statistical theory of the strength of materials. *Ingeniörvetenskapsakademiens Handlingar* 151:1-45.

Weibull W. 1951. A statistical distribution function of wide applicability. *J Appl Mech ASME* 18: 293-7.

Williams, J.H. & Johnson, C.D. 2004. Acoustic and optical borehole-wall imaging for fractured-rock aquifer studies. *Journal of Applied Geophysics* 55(1-2): 151-159.

Yi, C., Johansson, D., Nyberg U., Castedo, R., Natale, M., Santos, T., Segarra, P. & Sanchidrián, J.A. 2018. Fragmentation prediction: numerical modelling. *SLIM Deliverable Report D2.4*, European Union's Horizon 2020 research and innovation program, Grant agreement no. 730294.